J. Fluid Mech. (2007), *vol.* 593, *pp.* 475–504.
doi:10.1017/S0022112007008932 Printed in the United Kingdom

Increased mobility of bidisperse granular avalanches

ESPERANZA LINARES-GUERRERO, CELINE GOUJON AND ROBERTO ZENIT

Instituto de Investigaciones en Materiales, Universidad Nacional Autónoma de México, Apdo. Postal 70-360, México D.F. 04510, México

(Received 5 December 2006 and in revised form 3 September 2007)

The unexpected behaviour of long-runout landslides has been a controversial subject of discussion in the geophysics community. In order to provide new insight into this phenomenon, we investigate the apparent reduction of friction resulting from the presence of a second species of smaller particles in the bulk of the granular material that forms the avalanche. Results obtained by means of a two-dimensional soft particle discrete element numerical simulation are presented. The numerical experiments consider an avalanche of two-size particles, originally placed over an inclined plane. The friction coefficient for the particle–particle and wall–particle contacts is held fixed. The granular mass is allowed to evolve with time, until it comes back to rest on a horizontal plane. The position of the centre of mass is located, such that the runout length L_{cm}/H_{cm} could be measured, with L_{cm} and H_{cm} being the horizontal distance travelled and the height lost by the avalanche centre of mass, respectively. Many simulations were performed keeping the area of the avalanche constant, varying only the area fraction of small particles. The results show that the runout length increases with the area fraction of small particles, reaching a maximum for a given area fraction of small particles. A detailed analysis of the particle distribution in the granular mass indicates that the apparent friction coefficient is affected by the formation of a layer of small particles at the base of the avalanche. This layer is identified as the source of 'lubrication'. Furthermore, since there is a dependence of the runout on the fall height and the volume in real avalanches, some simulations with different areas and different fall heights were performed. The results show a tendency of the runout to increase with area, and to decrease with the initial fall height, which is in agreement with what is observed for geological events.

1. Introduction

The origins of the small apparent friction observed in long-runout landslides have long been the subject of speculation. Long-runout landslides consist of large masses of rock (of the order of a cubic kilometre of volume), the initiation of which could be the result of an earthquake. The runout distances of these events may cover many kilometres and have potential implications to human life and safety. Such events include different granular mass flows, such as rock avalanches, debris flows and pyroclastic flows. That is why the general term 'landslide' has been used by many authors to describe them. The term 'landslides' has been defined as a 'general term covering wide variety of mass movement ... involving ... downslope transport, by means of gravitational stresses of soil and rock material en masse' (Gary, McAffe &

Wolf 1972) . The term 'avalanche' has also been suggested to describe this phenomenon (Howard 1973), and it is usually used to refer to a dry granular mass flow. Bates & Jackson (1962) stretched the definition to include a fallen rock mass and associated motion. In this paper, we refer to the term avalanche since we consider a simplified case, where the effect of inter-granular fluid is negligible so the granular mass is not cohesive.

Many hypotheses have been put forward to explain the long runout. They are briefly summarized below, but also see Shaller & Smith-Shaller (1996). Some models have invoked the presence of a fluidizing medium such as air, water, vapour, volcanic gases or a suspension of fine particles (Legros 2002). Kent (1966) proposed that entrapped air could fluidize landslides. Shreve (1968) and Fahnestock & Voight (1978) suggested that a cushion of entrapped air would support landslides rather than fluidize them. Hsü (1975) hypothesized that the fine particles alone, without the help of a supporting fluid, could fluidize the coarser moving debris. On the other hand, some authors have attempted to explain landslide mobility with fluid-absent granular models. The proposed models include acoustic fluidization (Melosh 1979), spreading of a rapid granular flow (Davies 1982; Straub 1996), self-lubrication (Campbell 1989; Cleary & Campbell 1993), spreading of a granular flow in a regime transitional between frictional and collisional (Campbell, Cleary & Hopkins 1995), and the support of the avalanche over a thin collisional region of intense shear (Huppert & Dade 1998).

The mobility of landslides has also been considered using continuum models with bulk rheological properties such as viscosity and yield strength, without specific assumptions about the microscopic physics (Dade & Huppert 1998). Models which take into account changes of mass due to deposition or bulking have also been proposed (Hungr & Evans 1997). Studies which use monodisperse dry granular mass flows, show strong dependence of flow runout on the initial aspect ratio of the granular columns (Lajeunesse, Mangeney-Castelnau & Vilotte 2004; Lube *et al.* 2004; Balmforth & Kerswell 2005; Zenit 2005; Lajeunesse *et al.* 2006), challenging the traditional view that the extent of geophysical granular flows depends on their volume. Moreover, Phillips *et al.* (2006) found that for a given proportion of fine particles in a bidisperse avalanche, the mobility is larger. While many of the proposed mechanisms may have been relevant in specific landslides events, none of them has been widely recognized as a universal explanation for landslide mobility, and the debate continues.

In order to provide a new insight into this phenomenon, we investigate the apparent reduction of friction resulting from the presence of small particles. In this paper, we present an alternative explanation for the increased mobility of landslides. In general, landslides are composed of particles of many sizes. Although, the mechanics of polydispersed granular masses is far from being understood (Goujon, Dalloz-Dubrujeaud & Thomas 2007), we consider a simplified case: the motion of a mass composed of two particle species, of the same density and with a significant size difference; that is a bidisperse case. When a bidisperse granular mass is moving whether shaken by vibration or moving through an inclined plane, the phenomenon of segregation occurs. The mechanism of the segregation is still not completely understood; however, there are a number of mechanisms for the segregation of dissimilar grains in granular flows, including inter-particle percolation, convection (Ehrichs *et al.* 1995), inertia, collisional condensation (Jenkins 1998), particle density (Drahun & Bridgwater 1983), gravity-driven size-segregation by kinetic sieving (Bridgwater 1976; Savage & Lun 1988; Thornton, Gray & Hogg 2006), and diffusive remixing (Hsiau & Hunt 1993; Savage & Dai 1993; Dolgunin & Ukolov 1995; Gray

& Chugunov 2006) which are the dominant processes in dense granular free-surface flows. Rosato *et al.* (1987) and Jullien, Meakin & Pavlovitch (1992) suggested the percolation of the small beads in the layer of large beads as a mechanism for particle size segregation by shaking. In this model, the small particles go down through the empty spaces formed during the vibration. In that way, the large particles stay in the free surface. In a similar manner, when a mixture of different sized particles flows over an inclined plane, the segregation occurs almost immediately. However for two-dimensional experiments, the segregation is slower, leading to a double segregation (Rosato *et al.* 1987; Savage & Lun 1988; Vallance & Savage 2000) in which the different classes of particles are not totally separated along the flow. During the flow, the particles are moving constantly and empty spaces between the particles appear. The large particles may go down only in large empty spaces, while the small particles go down in small and large spaces. This asymmetry in the fluctuation of the particle movement generates the segregation (dynamic percolation). A quantitative model based on this idea, was propounded by Savage & Lun (1988). However, for certain experimental configurations, inverse segregation can be observed (Thomas 2000).

By means of discrete-element computer simulations, the effect of a second species of particles on the runout of avalanches is studied. In § 2, a brief description of the computational technique is shown and the parameters in this study are presented and discussed. Several techniques used to analyse the numerical results are presented in § 3. In §§ 4, 5 and 6, the results are presented and discussed. Finally, in § 7, a brief summary and general conclusions are presented.

2. Discrete-element simulation

2.1. *Simulation method*

Results obtained by means of a two-dimensional soft particle numerical simulation are presented. The discrete-element computer code used in this study was developed by Wassgren (1996), and was adapted to simulate bidisperse flows. This technique was first proposed by Cundall & Strack (1979) to study granular flows. A similar simulation scheme was used by Campbell *et al.* (1995) to study the mobility of large avalanches.

In this case, only gravity and contact forces are considered. Both the linear and angular momentum conservation equations are solved for each particle at every time step. The contact forces are modelled for both the normal and tangential directions.

The particle surfaces are allowed to overlap slightly in order to model elastic deformations (soft particle scheme). In the simulations used in this study, the maximum allowed overlap is 10% of the smallest particle diameter of the two particles in contact. For the normal direction, the linear hysteretic spring model proposed by Walton & Braun (1986) was used, which accounts for the collision energy loss using a spring with two different stiffnesses. The loading stiffness, k_L, is chosen to match Hertzian contact parameters; the unloading stiffness, k_U, is calculated from the loading stiffness and the coefficient of restitution, ϵ_n ($k_U = k_L/\epsilon_n^2$). For the tangential direction, a linear spring in series with the Coulomb sliding friction element model was used, as proposed by Cundall & Strack (1979). In this model, both forces (due to the slider and the spring) are calculated and the smallest value of these two is chosen. If the slider force is smaller than the spring force, then the two particles in contact are sliding over each other. The stiffness of the spring for tangential contact, k_S, is considered equal to the loading stiffness. The simulation time step is calculated in such a way that it is always smaller than the typical collision duration. As there

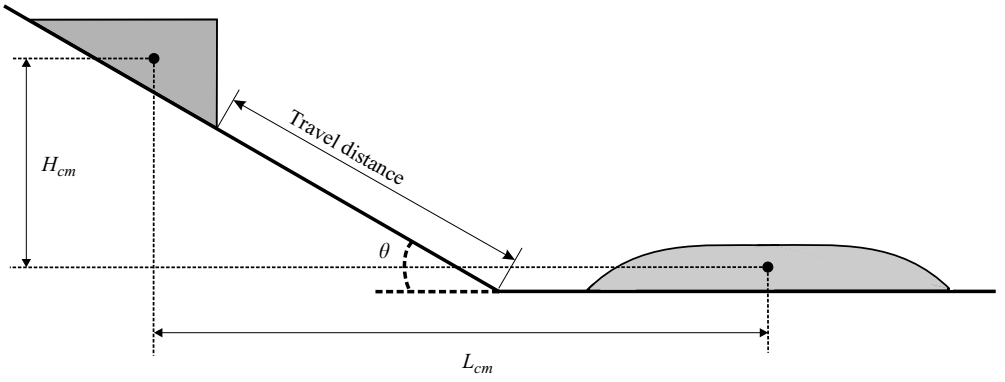

FIGURE 1. Sketch of initial configuration and final deposit. L_{cm} (resp. H_{cm}) is the horizontal (resp. vertical) distance between the two centres of mass of the deposit at the beginning and at the end of the simulation, ($\theta = 30°$).

are two kinds of contacts (translational and rotational), the smallest contact time is chosen. The simulation time step is at least ten times smaller than this minimum contact time which is calculated from the Hertz contact theory.

In a discrete-element simulation, the majority of the computational overhead is spent in checking the contact between particles. In order to reduce the number of collision checks of each particle, a neighbouring-cell technique was implemented in the simulation code. The details of the implementation of the code can be found in Wassgren (1996).

The validity of these types of model has been discussed extensively in the granular flow literature (see Rotter *et al.* 1998). For dense flows, in which the particle contacts are enduring, the hysteretic spring contact model can be considered to be the most appropriate since this approach leads to realistic impact behaviour, where it is assumed that in each time step, the normal force changes by only a small amount which will not significantly influence the tangential force. Results obtained using this model reproduce experimental values of individual particle collisions (Schafer, Dippel & Wolf 1996) and correctly predicts static pressures in silos (Rotter *et al.* 1998).

2.2. *Paramenters and numerical experiments*

The configuration studied here is shown schematically in figure 1. The numerical experiments consist of an avalanche of two species of particles, small particles with a diameter equal to d_s and large particles with a diameter equal to d_l, on a smooth frictional plane with an inclination, θ, of 30°. The diameter of large beads is the same for all the simulations, thus the diameter of small particles determines the diameter ratio, defined as d_l/d_s. The initial elevation was chosen such that the travel distance on the inclined plane is equal to 50 times the large-particle diameter. A dispersity of the particle size of $\pm 10\%$ around the mean value of the diameter is chosen in order to avoid crystallization. The coefficient of friction for the particle–particle and wall–particle contacts is held fixed and is equal to 0.5, a typical value of the frictional properties of rocks (Campbell 1989). The coefficient of restitution, ϵ_n, is equal to 0.2. The values of the loading stiffness were calculated according to the expression proposed by Zenit (2005):

$$k_L = \frac{2m^* g}{d^*} \frac{\dot{\alpha_0}}{\alpha_{max}} \exp\left(\frac{-\arctan\beta}{\beta}\right), \tag{2.1}$$

ν_s	d_l/d_s	n_l	n_s	n_{total}
0	–	500	–	500
0.5	8.33	250	17362	17612
0.5	4	250	4000	3500
0.5	3	250	2250	2900
0.5	2	250	1000	1250

TABLE 1. Number of small and large particles for different simulations. n_l (resp. n_s) is the number of large (resp. small) particles; n_{total} is the total number of particles.

where $m^* = m_l m_s/(m_l + m_s)$ and $d^* = d_l d_s/(d_l + d_s)$ are the equivalent mass and diameter, respectively, and $\beta = \pi/\ln \epsilon_n$. The terms $\dot{\alpha_0}$ and α_{max} are the maximum overlap and a characteristic collision speed. The values of k_L were in the range $1.5 \times 10^5 > k_L/(\rho d_s^2 g) > 1.9 \times 10^5$, corresponding to the chosen values of ϵ_n and d_l/d_s investigated here. The mass and the density of the particles were scaled and therefore will not affect the simulation results since only inter-particle contact and body forces are considered. All numerical quantites were made dimensioless considering d_s, g and ρ as the characteristic scales.

The simulation parameters are the total area occupied by the beads, the initial position of the avalanche, the diameter ratio (d_l/d_s) and the area fraction of small beads (ν_s) defined by:

$$\nu_s = A_s(A_s + A_l)^{-1}. \tag{2.2}$$

where A_s is the total area of small particles, and A_l is the total area of large particles.

In this investigation, three different kinds of simulation were performed. In the first one, the total area occupied by the particles remains constant, varying only the diameter ratio d_l/d_s (from 1.5 to 8.33) and the area fraction of small particles ν_s (from 0 to 1). The total area occupied by the beads corresponds to the area occupied by 500 large beads. If the diameter of large beads is equal to 1 m in dimensional units then the avalanche area is equal to 392.7 m^2. The number of particles in each simulation depends on the diameter ratio and the area fraction of small particles. The number of small particles is given by $n_s = \nu_s n_o (d_l/d_s)^2$, where n_o is the number of large particles for a simulation with a $\nu_s = 0$. Table 1 shows n_s for some simulations. The largest case was for a monodispersed simulation ($d_l/d_s = 8.33$ and ν_s=1) with 48 000 particles, which ran for approximately one month in a Pentium IV PC. For each case, simulations were run from 1 to 5 times, with slightly different initial conditions to ensure repeatability.

The second type of simulation considers avalanches with a constant area but with different initial fall heights, corresponding to travel distances varying from $20d_l$ to $300d_l$. Lastly, the influence of the avalanche area on the global coefficient of friction was studied in a third type of simulation. These simulations were run for constant diameter ratio and the area fraction of small beads are constant ($d_l/d_s = 3$ and $\nu_s = 0.6$), varying only the area of the avalanche from 5000 to 40 000 dimensionless area units ($4A_{tot}/(\pi d_s^2)$).

The initial bulk avalanche is prepared by filling a box formed by three walls with the two species of particles (figure 2). In the initialization, the particles are located randomly (figure 2*a*), leading to a relatively well-mixed avalanche initial bulk (see § 3.3). The particles settle during the initialization step (figure 2*b–d*) until their kinetic energy is dissipated and the initial deposit is formed (figure 2*e*). When the particles

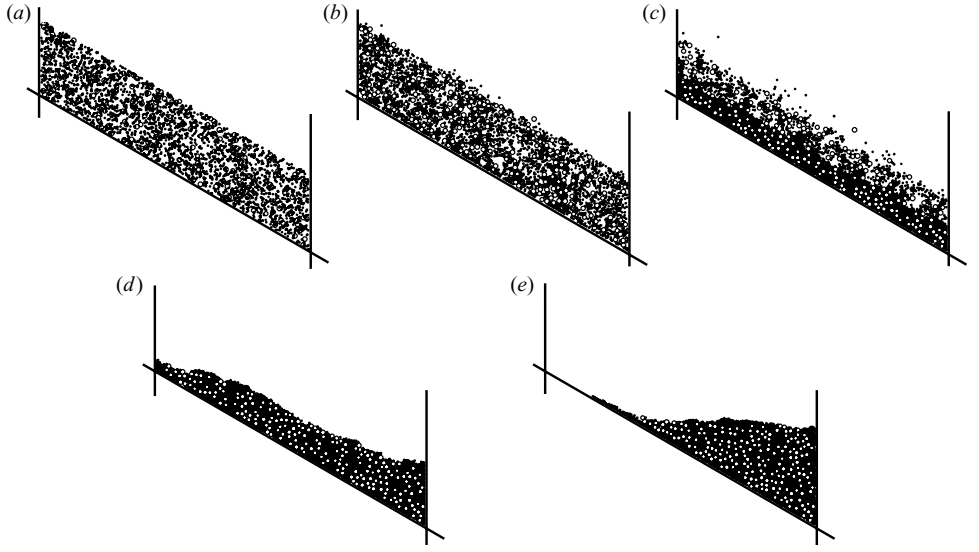

FIGURE 2. Snapshots of the initialization simulation for different dimensionless times: $t^* = t\sqrt{g/d_s}$, (*a*) random particle locations $t^* = 2$, (*b*) $t^* = 8$, (*c*) $t^* = 14$, (*d*) $t^* = 28$ and (*e*) $t^* = 60$, ($d_l/d_s = 3$, $\nu_s = 0.6$).

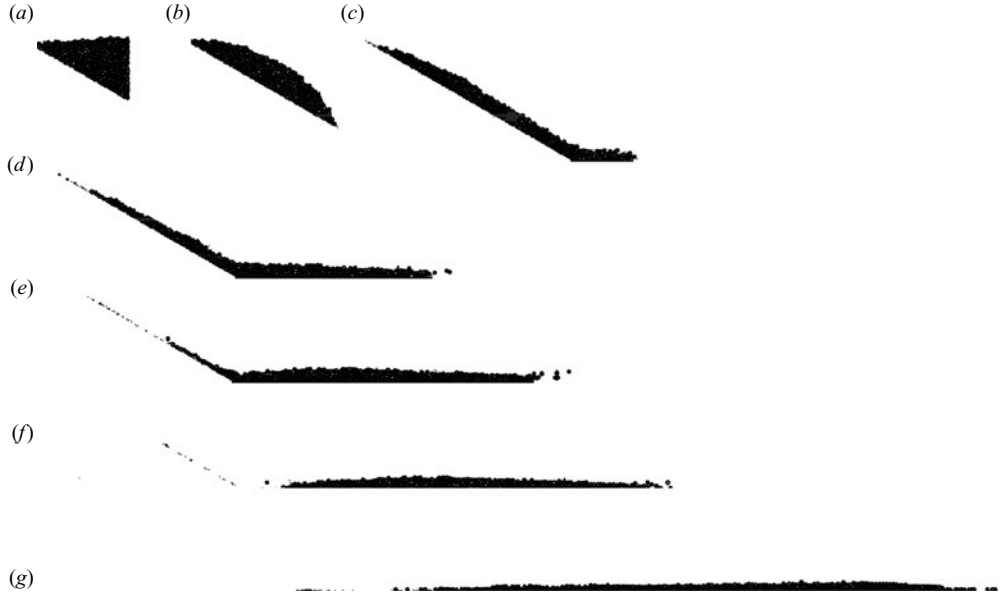

FIGURE 3. Moving of the bidisperse granular mass along the plane for different dimensionless times $t^* = t\sqrt{g/d_s}$. (*a*) $t^* = 0$, (*b*) $t^* = 20$, (*c*) $t^* = 40$, (*d*) $t^* = 60$, (*e*) $t^* = 80$, (*f*) $t^* = 100$, (g) $t^* = 250$ (end of the simulation); ($d_l/d_s = 8.3$, $\nu_s = 0.25$).

are at rest, the vertical wall that keeps the avalanche from moving down the slope is removed. Figure 3 shows a typical evolution of a simulation for different dimensionless time instants, $t^* = t\sqrt{g/d_s}$. The granular mass falls down over the smooth-frictional inclined plane, under the influence of the acceleration due to gravity g, the granular mass accelerates, reaches the horizontal plane (also smooth but frictional) and then slows down along the horizontal plane, until it comes back to rest.

3. Data analysis

Since literally everything about the simulated system is accessible, valuable information can be obtained by further analysing the numerical results. In this section, several analysis tools and calculations are briefly described.

3.1. *Global friction coefficient and kinetic energy*

Large rock avalanches are commonly described by their relative runout length defined as the ratio of the total drop height, H_{max}, and the runout distance, L_{max} (Shreve 1968). The application of this ratio to calculate the equivalent coefficient of friction entails the centre of mass of the fallen mass being shifted from the highest point on the initial position to the furthest point of the avalanche. Physically, the line connecting these two points is not the line connecting the centre of mass of the initial maximum drop height and the avalanche final deposit. Therefore this assumption is inaccurate. Thus, the parameters of interest are the centre of mass of the initial and the final avalanche deposit, that is H_{cm} and L_{cm}. Hence, we define the global friction coefficient of the avalanche to be:

$$\mu = \frac{H_{cm}}{L_{cm}}. \tag{3.1}$$

By locating the position of the centre of mass of the avalanche, the runout length L_{cm} and the total drop height H_{cm} can be measured. The height is then

$$H_{cm} = |y_{cm,final} - y_{cm,initial}|,$$

and the runout length is

$$L_{cm} = |x_{cm,final} - x_{cm,initial}|,$$

where $(x_{cm,initial}, y_{cm,initial})$ and $(x_{cm,final}, y_{cm,final})$ represent the coordinates of the centre of mass for the initial and final times, respectively.

For a few well-documented deposits, this ratio can be estimated with some confidence. The data report low values of H_{cm}/L_{cm}, showing that the centre of mass travels further than predicted by a frictional model with a constant friction coefficient. The use of this ratio as an indicator of landslide mobility implies that the energy released during the initial fall is dissipated with a constant coefficient of friction and is responsible for the runout distance (Legros 2002).

The kinetic energy associated with the translational motion is $E_k = 1/2 \sum_i m_i v_i^2$, where m_i is the mass and v_i is the magnitude of the translational dimensionless velocity of the particle i defined as $v_i = (v_{xi}^2 + v_{yi}^2)^{1/2}$ where v_{xi} (resp. v_{yi}) is the horizontal (resp. vertical) velocity. The dimensionless kinetic energy is defined as the ratio of the translational kinetic energy and the initial potential energy.

3.2. *Measurement of particle concentration*

The particle concentration, or compactness, can be measured directly from the simulation results. The compactness for each bead on the granular mass was calculated using Voronoï cells (Barber, Dobkin & Huhdanpaa 1996). With this technique, details of which can be found in the reference, the space around each particle can be calculated; therefore, the area fraction for each particle is inferred as the ratio of the particle area to the total area (space plus particle). A measurement of the compactness, for layers or for the total mass, can then be obtained. Figure 4 shows an example of the Voronoï calculation used in this study.

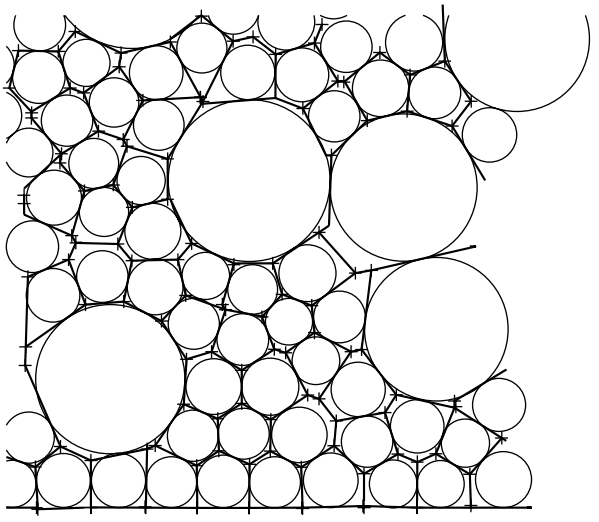

FIGURE 4. Example of Voronoï cell calculation. For this case, $dl/ds = 3$, $\nu_s = 0.25$. The measured mean compactness is equal to 0.68.

3.3. *Measurement of particle segregation*

The most difficult issue to tackle in the study of size segregation in granular flows is its quantification. Experimentally, segregation in avalanches is drastic: particles of the same size migrate to the same region, separating completely from the rest (Goujon *et al.* 2007). For two-dimensional flows, the size segregation is not efficient and it is possible to observe double segregation (Rosato *et al.* 1987; Savage & Lun 1988; Vallance & Savage 2000). Therefore, it is not clear how to determine the degree of mixing or segregation from simple inspection.

We propose a new technique to characterize particle segregation. It considers the calculation of Lorenz curves and Gini coefficients. These mathematical tools are widely used in the field of econometrics to quantify the distribution of wealth (Gastwirth 1972). A description of how to adapt these tools to study particle segregation in granular flows is shown below.

3.3.1. *The Lorenz curve and Gini coefficient as a measure of particle segregation*

The Lorenz curve (Lorenz 1905) is a graphical representation of the cumulative distribution function of a probability distribution. It is often used to represent income distribution. For instance, consider the $x - y$ plot in figure 5. The x-coordinate shows the bottom x-percentage of households and y is the percentage of the total income that they have. Every point of the Lorenz curve represents a statement such as 'the bottom 20% of all households have 10% of the total income'. A perfectly equal income distribution would be one in which every household has the same income. This can be depicted by the straight line $y = x$. By contrast, a perfectly unequal distribution would be one in which one person has all the income and everyone else has none. This curve is called the line of perfect inequality. The Gini coefficient (Gini 1912) is a measure of the inequality of a distribution. It is defined as the area between the line of perfect equality and the Lorenz curve, with values between 0 and 1 representing perfect equality and inequality, respectively.

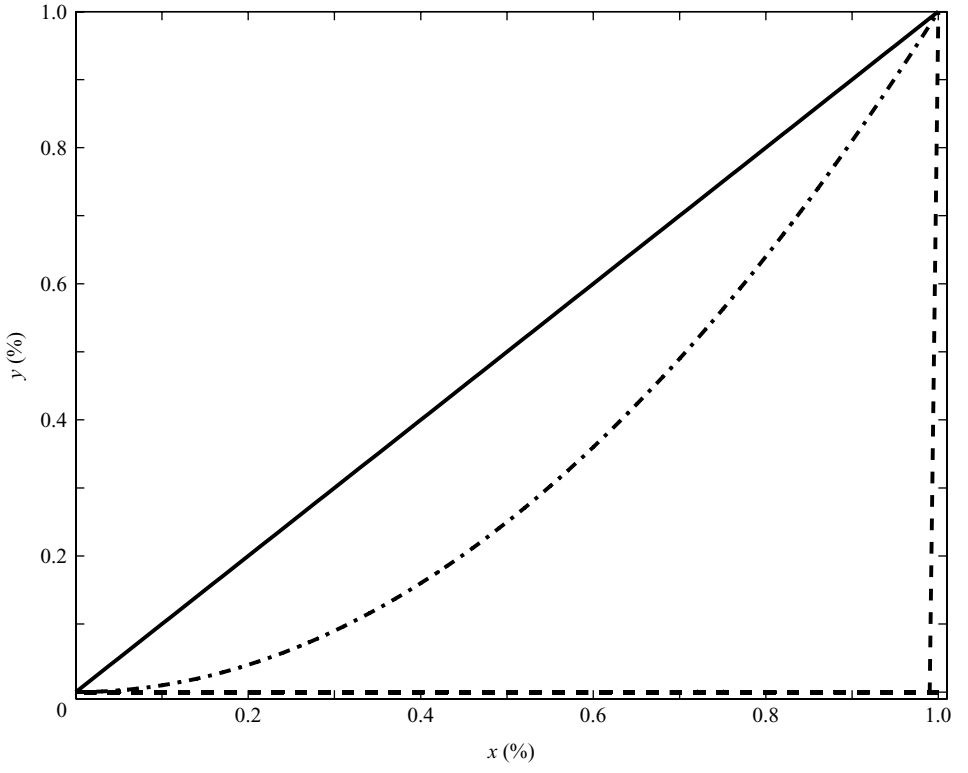

FIGURE 5. Typical Lorenz curve (dashed-dotted line). Curves representing perfect equality and inequality are also shown (continuous and dashed lines, respectively).

The Lorenz curve and the Gini coefficient can be used to characterize the segregation in bidisperse flows. For this, we determine the area of the small and large particles in different layers of the flow. The thickness of the layers is an arbitrary parameter, but it can be shown that for layer thicknesses smaller than $d_s/2$, the measure is independent of this choice.

The cumulative percentage of the area of small beads present in each layer can be calculated as

$$L_s(y) = \frac{Area_s(y)}{Area_s}, \tag{3.2}$$

where $Area_s(y)$ is the area of small beads in the layer at depth y, and $Area_s$ is the total area of small beads in the avalanche. For the large particles, $L_l(y)$ can be calculated in the same manner. Hence, the Lorenz curve is the graphical representation of L_s or L_l as a function of y/y_{max} shown in percentages. A Lorenz curve closer to the perfect equality (straight line at 45°) would, therefore, represent a well-mixed granular mass.

The Gini coefficient for small particles is calculated as

$$G_s = 1 - 2\int_0^1 L_s(y^*)\,\mathrm{d}y^*, \tag{3.3}$$

where $y^* = y/y_{max}$. The corresponding Gini coefficient for large particles, G_l, is calculated in a similar manner. A Gini coefficient close to zero would represent a well-mixed granular mass, whereas a value close to 1 would indicate a completely segregated state.

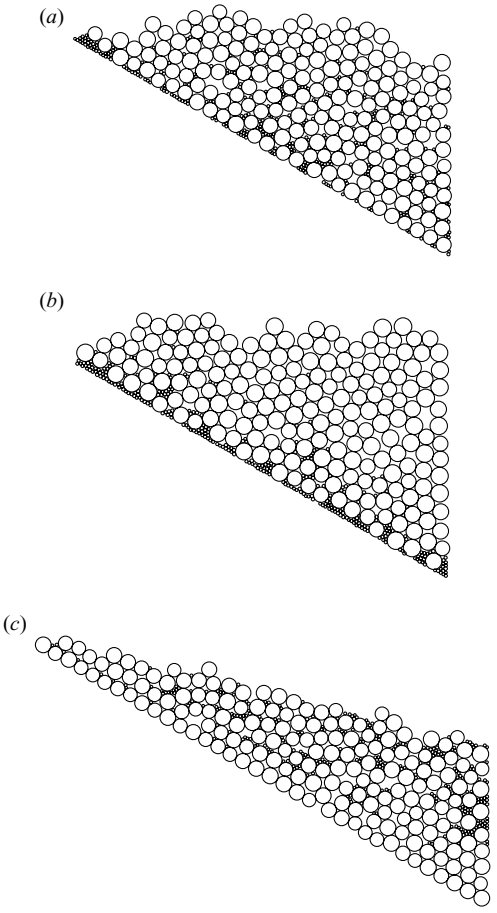

FIGURE 6. Three different initial configurations: (*a*) a nearly homogeneous mixture; (*b*) the small beads are at the base of the flow; (*c*) the small beads are at the top of the flow. For all cases $d_l/d_s = 5$ and $\nu_s = 0.20$.

Figure 6 shows three different initial deposits, which were prepared in different ways to study the influence of the initial distribution of particles on the avalanche runout. This is described in more detail in the Appendix. The first deposit was prepared in the same way as all other tests in this investigation; that is, particles are relatively well mixed initially. For the second and third cases, the small particles were placed at the bottom or top of the initial region, respectively, to have a preferential distribution.

Figure 7 shows the calculated Lorenz curves and Gini coefficients for the three deposits shown in figure 6. The solid and dashed lines show Lorenz curves for the small and large particles, respectively, for each case. In the well-mixed case (*a*), the Lorenz curve for small beads is slightly below than that for large beads, which denotes a slight segregation. Case (*b*) shows also that the Lorenz curve for small beads is below that for large beads, but the difference is more important than in the previous case. Hence, the segregation is stronger. Also, the calculated Gini coefficient for small beads is larger than the previous case. On the other hand, case (*c*) shows that the Lorenz curve for small beads is above that for large beads. This is an indication that the particles are segregated, but the small ones are on the top of the mass. Note that for this case, the Gini coefficient is also smaller than that for case (*a*).

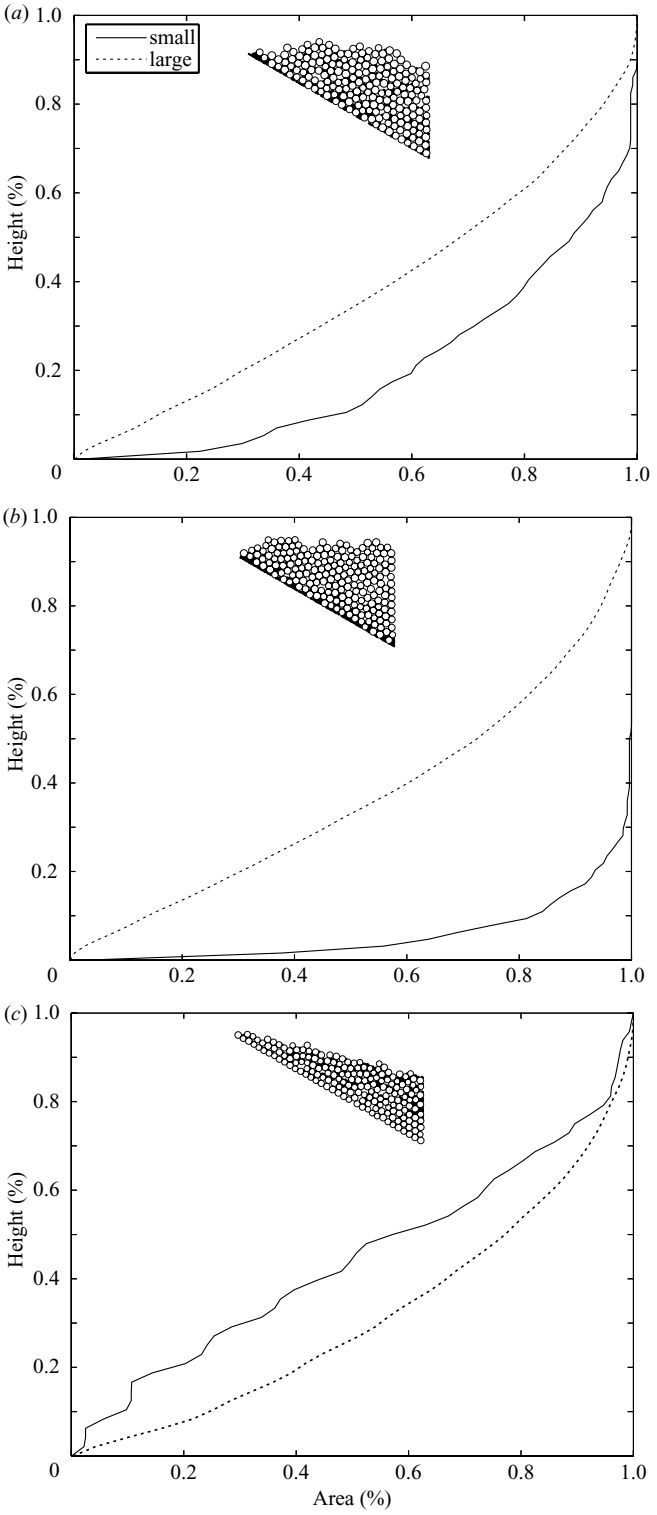

FIGURE 7. Lorenz curves for the three initial configurations shown in figure 6. The solid and dotted lines correspond to large and small particles, respectively. (*a*) $G_s = 0.56$, (*b*) 0.86, (*c*) 0.12.

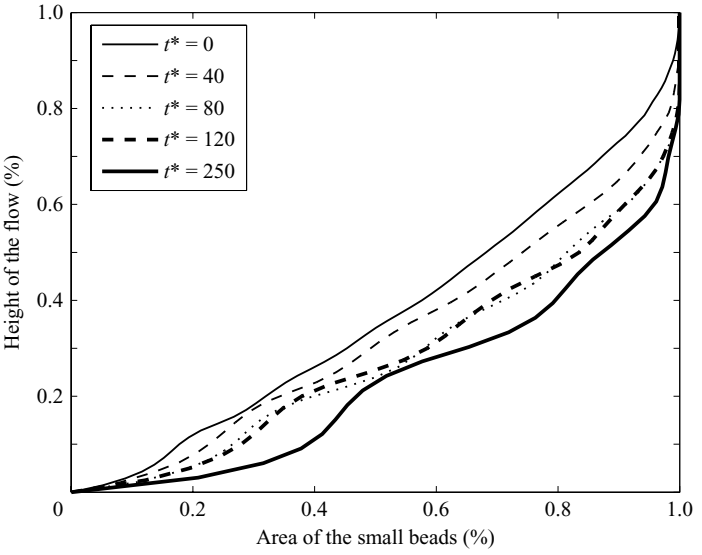

FIGURE 8. Lorenz curves for $d_l/d_s = 8.3$ and $\nu_s = 0.25$ for different dimensionless times. (*a*) Initial distribution, $t^* = 0$, $G_s = 0.37$; (*b*) $t^* = 40$, $G_s = 0.35$; (*c*) $t^* = 80$, $G_s = 0.44$; (*d*) $t^* = 120$, $G_s = 0.44$; (*e*) $t^* = 250$, $G_s = 0.54$.

4. Bidispersity effect on runout extent

4.1. *Segregation and compactness*

Because of the difference in size of the two classes of particles, segregation occurs during the avalanche: small particles move down during the flow. Since the coefficient of friction is the same for small and large particles, the segregation is only a result of geometrical effects. The segregation can be assessed with the Lorenz curves. Figure 8 shows the Lorenz curves for different time instants during the evolution of the avalanche, for a typical case ($d_l/d_s = 8.3$, $\nu_s = 0.25$). It can be noted that the area fraction of the small beads at the base of the flow is increasing with time, which means that segregation is occurring and that it progresses with time. Moreover, during the avalanche, it is possible to distinguish three regions: a layer composed of only small particles at the base of the flow; a layer composed of a mixture of the two species of particles in the middle of the flow; and depending on the area fraction of small particles, a layer composed of only large particles (small values of ν_s), or a layer composed of only small particles (large values of ν_s) at the top of the flow.

It is also possible to determine the efficiency of the segregation for each diameter ratio. For this, the Lorenz curve is calculated for different diameter ratios with the same area fraction of small beads for the final deposit (figure 9). It is clear that the degree of particle segregation increases with diameter ratio.

Figure 10 shows the mean compactness of the avalanche, measured using Voronoï cells, as a function of time for each particle size ratio. In all cases, the compaction initially decreases, during the acceleration part of the avalanche when the mass is still over the inclined plane. A minimum compaction is found when the bulk of the avalanche passes from the inclined to the horizontal plane. Subsequently, the concentration increases to reach a nearly constant value. It is important to note that in all cases the mean compactness is larger than 0.61. For such values of the

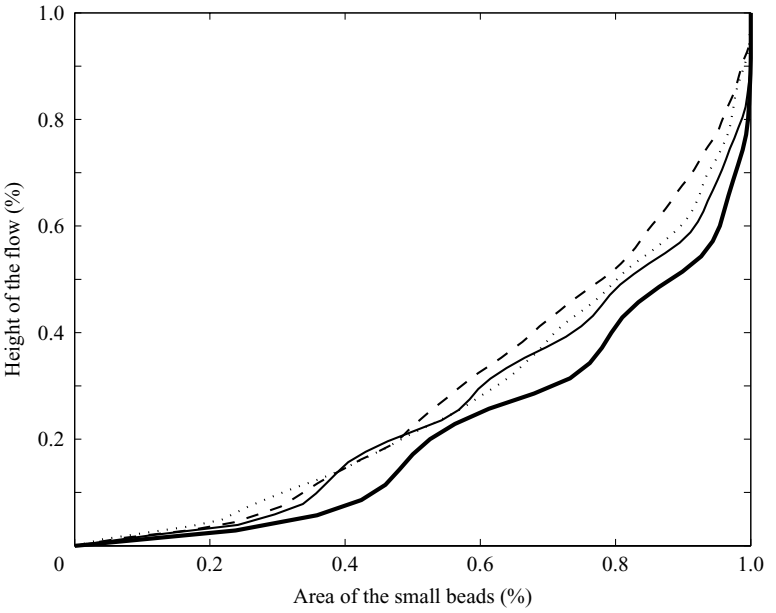

FIGURE 9. Lorenz curves for $\nu_s = 0.25$ and for different diameter ratios. (*a*) $d_l/d_s = 8.33$ (solid thick line), $G_s = 0.57$; (*b*) $d_l/d_s = 4$, (solid thin line), $G_s = 0.48$; (*c*) $d_l/d_s = 3$, (dotted line), $G_s = 0.42$; (*d*) $d_l/d_s = 2$, (dashed line), $G_s = 0.42$.

compactness, flows influenced by gravity can be considered dense, for which enduring contacts are dominant and few collisions occurs.

4.2. *Global friction coefficient*

Figure 11 shows the global friction coefficient as a function of the area fraction of small particles ν_s, for different size ratios. For avalanches with $\nu_s = 0$ and $\nu_s = 1$, that is for mono-dispersed flows, the global friction coefficient μ is slightly smaller than the value of the coefficient of friction used in the simulation (0.5).

For size ratios larger than 2, the global friction coefficient decreases with the area fraction of small particles. For a certain area fraction of small particles $\nu_{s,m}$, the global friction coefficient is minimum. For area fractions of small particles larger than $\nu_{s,m}$, the global friction coefficient μ increases with the area fraction of small beads. In figure 12, the area fraction for which the runout is the longest is shown as a funtion of particle diameter ratio, d_l/d_s. We can also observe that the area fraction of small beads for which the friction is minimum, decreases monotonically with the size ratio.

On the other hand, for a size ratio smaller than or equal to 2, the global friction coefficient was found to be nearly constant, slightly larger than the value for mono-dispersed flows. No minimum effective friction coefficient was found for the whole range of ν_s.

4.3. *Evolution of kinetic energy of the avalanche*

The existence of an area fraction for which the global coefficient of friction is minimum can be related to the evolution of the translational kinetic energy. In figure 13, the variation of the dimensionless kinetic energy is presented for a size ratio equal to 8.33 and for different area fractions of small beads. For the area fraction of small beads equal to 0.25, which approximately corresponds to the area fraction for which the global friction coefficient is minimum, the kinetic energy is maximum. The

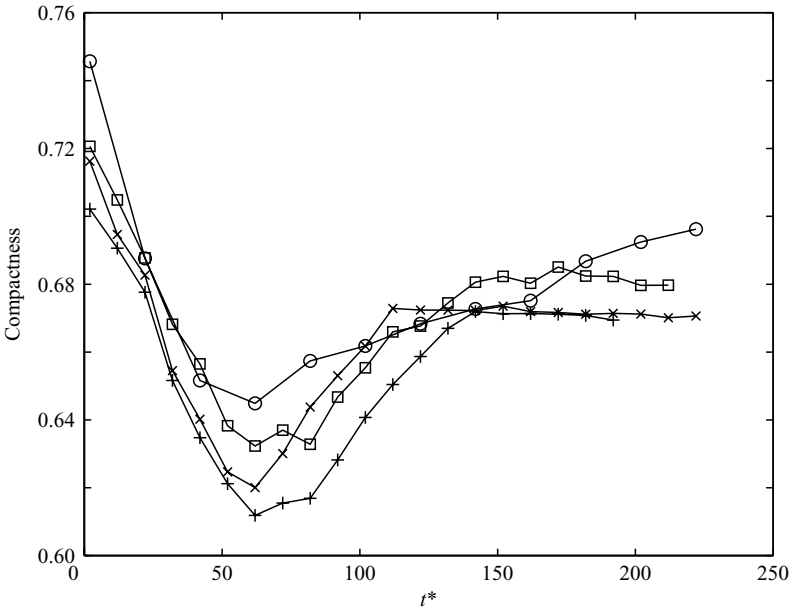

FIGURE 10. Mean compactness of the avalanche as a function of dimensionless time for four different particle size ratios. (*a*) $d_l/d_s = 8.33$ (○); (*b*) $d_l/d_s = 4$ (□); (*c*) $d_l/d_s = 3$ (×); (*d*) $d_l/d_s = 2$ (+). For all cases $\nu_s = 0.25$.

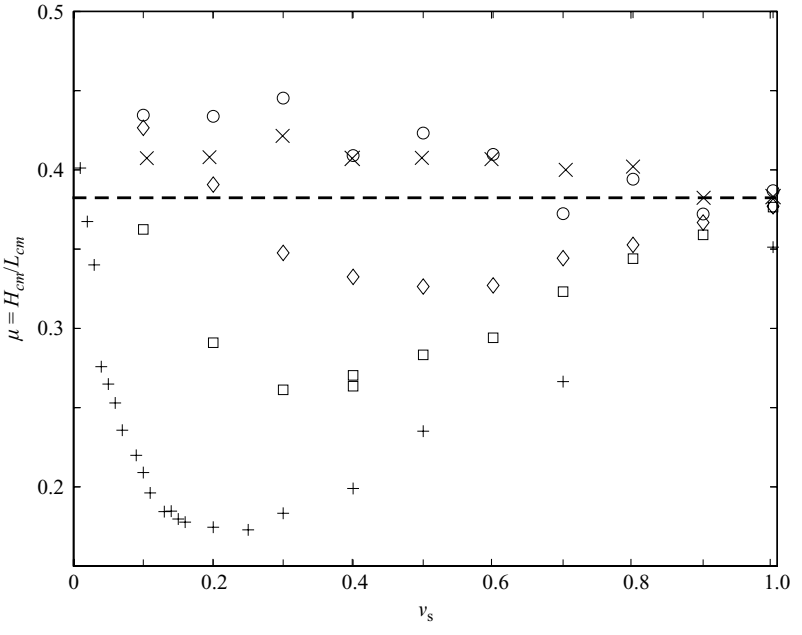

FIGURE 11. The global friction coefficient $\mu = H_{cm}/L_{cm}$ as a function of the area fraction of small particles ν_s for different ratios: +, $d_l/d_s = 8.33$; □, $d_l/d_s = 4$; ◇, $d_l/d_s = 3$; ○, $d_l/d_s = 2$ and ×, $d_l/d_s = 1.5$. The dotted line represents the value of the global friction coefficient for monodisperse flows. An area fraction of small particles for which the global friction coefficient is minimum appears for size ratios larger than 2.

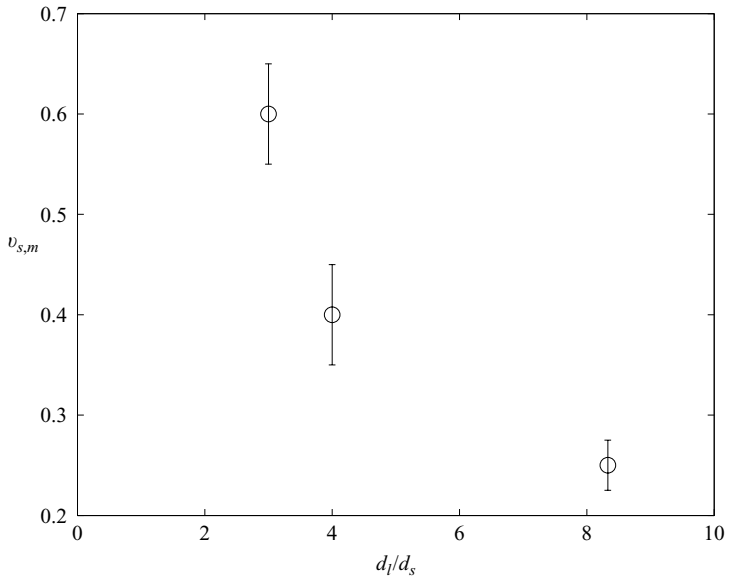

FIGURE 12. Area fraction of small beads for which the minimum friction is obtained, $v_{s,m}$ as a function of diameter ratio d_l/d_s.

behaviour of the dimensionless kinetic energy is similar for simulations with diameter ratios larger than 2. Moreover, the maximum of the kinetic energy increases with the diameter ratio as shown in figure 14. Hence, the maximum of the dimensionless kinetic energy is larger for lower values of the global friction coefficient.

For a diameter ratio smaller than 2, the behaviour of the dimensionless kinetic energy is not the same as the one presented for larger diameter ratios. As can be seen in figure 15, the curves of the dimensionless kinetic energy are not classified: the maximum of the dimensionless kinetic energy fluctuates with an increase of the area fraction of small beads. It is not evident, as in the other cases, that a maximum of the dimensionless kinetic energy is related to a minimum of the global coefficient of friction. However, the relation between the global friction coefficient and the kinetic energy remains since the larger values of the dimensionless kinetic energy correspond to the area fraction of small particles for which the global friction coefficient is small ($v_s = 0.7$ and $v_s = 0.9$ for the case of $d_l/d_s = 2$).

4.4. *Lubricant basal layer of small beads*

The minimum of the global friction coefficient can be explained by analysing the distribution of particles in the bulk of the avalanche. In particular, as will be shown, the lubrication appears when a layer of small beads forms at the base of the flow.

In figure 16, the distribution of the particles around the centre of mass of the final deposit is shown, for different diameter ratios and different area fractions of small beads. The formation of a layer at the base of the flow composed by small particles can be observed (shaded particles). This layer is identified by determining the small particles that are beneath large particles with a minimum height throughout the final deposit. For that, a contour under such large particles is defined (figure 17). The layer is identified by counting the small particles which are beneath the contour. As shown in figure 16(*b–d*), for size ratios larger than 2, for small v_s, the layer of small particles at the base of the flow is not continuous owing to the presence of some large beads

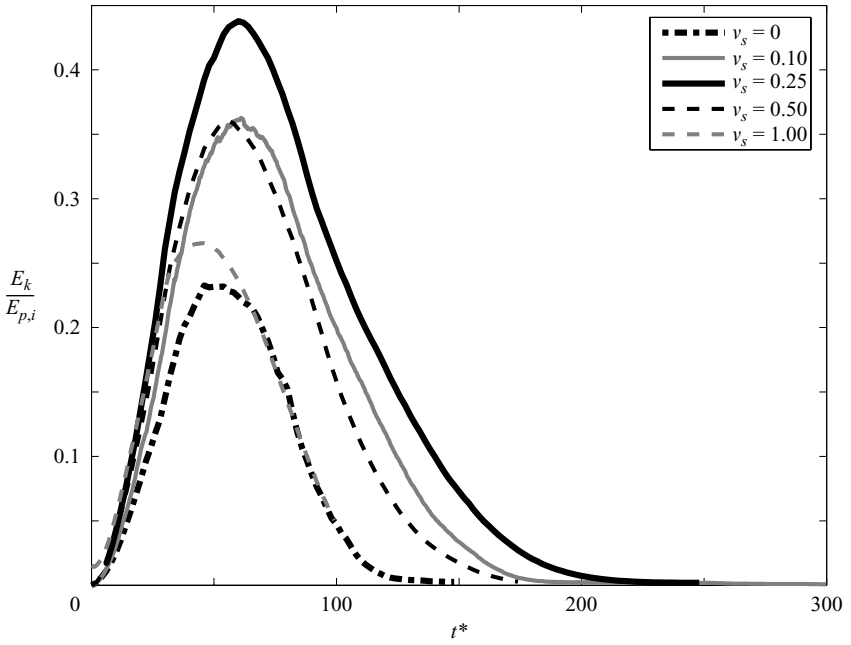

FIGURE 13. The translational kinetic energy E_k divided by the initial of the potential energy $E_{p,i}$ as a function of the dimensionless time t^* for different area fractions of small particles for the ratio $d_l/d_s = 8.3$. The area fraction of small particles for which the kinetic energy is maximum corresponds to that for which the global friction coefficient is minimum.

at the base of the deposit. For $\nu_s \simeq \nu_{s,m}$, the layer of small particles is continuous throughout the deposit. For large ν_s, the thickness of the layer of small particles at the base of the flow is thicker. On the contrary, as shown in figure 16(*a*), for the case of $d_l/d_s = 2$, there is no area fraction of small beads for which there is a continuous layer of small particles at the base of the flow.

This analysis suggests that not only the continuity of the basal layer characterizes the final deposit distribution for cases in which the minimum friction was observed; the height of the basal layer is also important. To measure the thickness of this basal layer, its height was calculated as follows: the final deposit length L was determined without taking into account the sparse particles that rolled individually in the extreme sides of the deposit. The small particles of the basal layer throughout the length L were identified. The area occupied by these particles divided by their compactness were considered equal to the height of the layer h_{layer} multiplied by L. Therefore:

$$h_{layer} = \frac{\pi \sum_{i=1}^{n} d_i^2}{4CL}, \tag{4.1}$$

where n is the number of small particles at the basal layer throughout the length L and C is the compactness. The compactness, or area fraction, was measured to be equal to 0.78, in accordance to the value reported by Lun & Bent (1994) and Aharonov & Sparks (1999). Since the height of the layer would depend on the length L, the calculation of the effective height was made for different values of L (figure 17).

In figure 18, the thickness of the layer at the base of the flow for different diameter ratios is presented. The thickness is divided by the diameter of the small beads d_s.

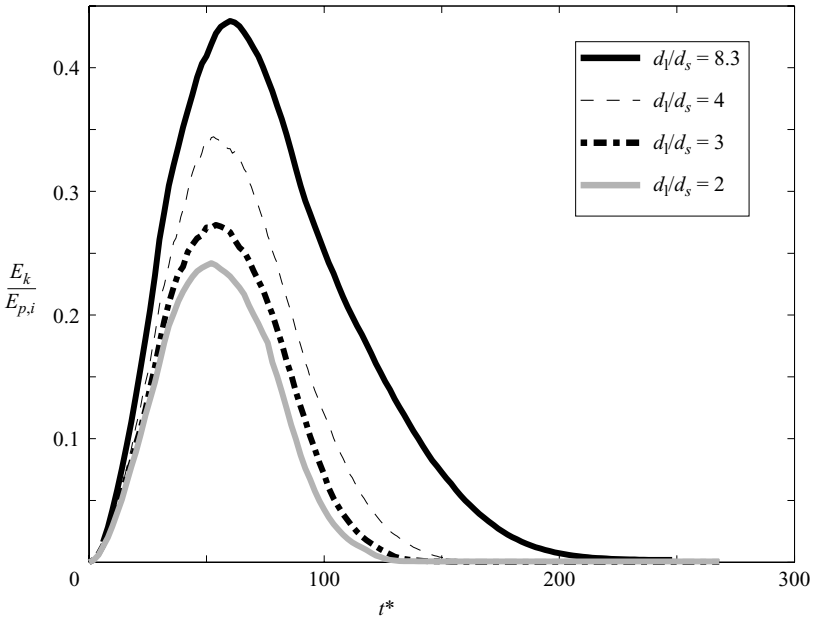

FIGURE 14. The dimensionless kinetic energy $E_k/E_{p,i}$ as a function of dimensionless time t^* for different diameter ratios for the critical area fraction of small particles ($\nu_{s,m}$) for which the global friction coefficient is minimum. The dimensionless kinetic energy increases with the diameter ratio.

For h_{layer}/d_s equal to 1 (horizontal dashed line), the area fraction of small particles is, in fact, that for which the global friction coefficient was found to be minimum. This is the case for all the diameter ratios.

With these results of the repartition of the small particles at the base of the flow, we can conclude that the maximum of the lubrication (which corresponds to a minimum of the global friction coefficient) is due to the formation of a continuous thin layer of small particles at the base of the deposit. The lubrication is most efficient when the layer is continuous and with a height aproximately equal to $1d_s$. The same qualitative behaviour was found by Siavoshi, Orpe & Kudrolli (2006) for the case of granular sliders.

4.5. *Rolling motion at the base of the flow*

From the results shown above, we can argue that the increased mobility of the avalanches is the result of the formation of a thin layer of small particles which changes the frictional dynamics at the base of the flow from sliding to rolling. To evaluate this argument, the average dimensionless angular velocity of the small particles in the basal layer was measured during the avalanche. For comparison, for ν_s equal to 0, the dimensionless angular velocity of large particles that were touching the plane was measured. The rotation is defined to be positive in the clockwise sense. The dimensionless angular velocity is defined as $\omega = \omega_z\sqrt{d_s/g}$, where ω_z is the particle rotational speed.

In figure 19, the variation of the average angular velocity for a diameter ratio equal to 8.3 is shown. It can be observed that for the critical area fraction of small beads ($\nu_s \approx 0.25$) the angular velocity is maximum. The rotation of the small beads increases with time, reaches a maximum value, and then decreases. The maximum of

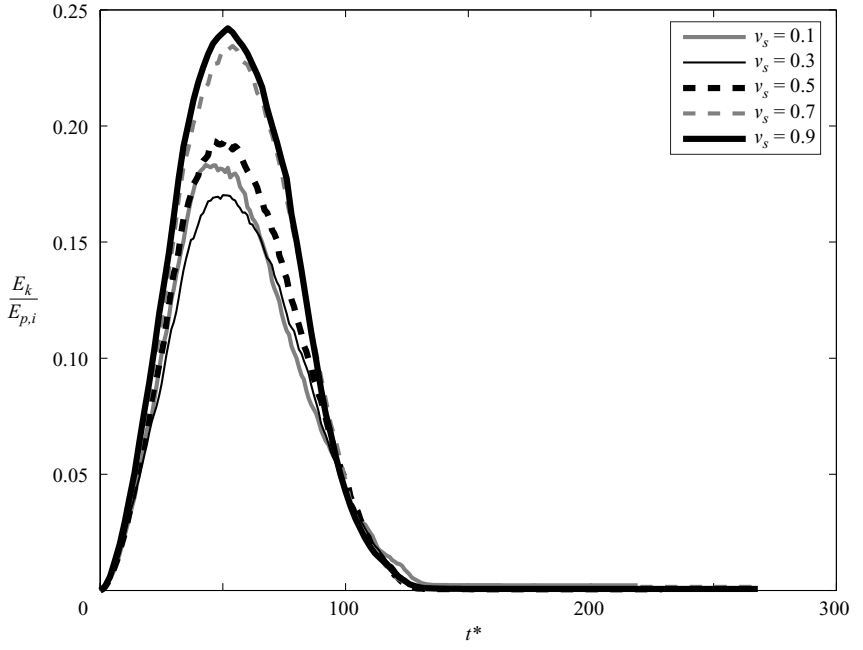

FIGURE 15. The dimensionless kinetic energy $E_k/E_{p,i}$ as a function of dimensionless time t^* for a diameter ratio equal to 2 for different area fractions of small particles (ν_s).

the rotation varies in the same way as the dimensionless kinetic energy: the maximum of the rotation increases with the area fraction of small beads, and it is maximum for the area fraction of small beads for which the global coefficient of friction is minimum, and for the area fraction of small beads larger than this critical value, the maximum of the rotation decreases with the area fraction of small beads. This behaviour of the variation of the angular velocity is similar for all the diameter ratios larger than 2. Moreover, the rotation increases with the diameter ratio as shown in figure 20.

These results indicate that the presence of the small particles at the base of the flow result in an increase of the rolling-type interactions with the plane which, in turn, lead to a reduction of the global friction of the avalanche.

In summary, the minimum of the global coefficient of friction is linked to the maximum of the dimensionless kinetic energy. The minimum of the global coefficient of friction can be explained by the formation of a layer of small beads at the base of the flow. The coefficient of friction is minimum for a thickness of the layer of small beads equal to d_s and with a large value of the rotation of these small beads. This layer of small beads can be identified as the source of 'lubrication'. In the following, we present the results concerning the influence of the initial position and the area of the avalanche on the global coefficient of friction.

5. Dependence of runout on initial bulk height

Legros (2002) proposed that the runout distance does not depend on fall height, and that it only adds scatter to the correlation between the ratio H_{cm}/L_{cm} and the landslide volume. On the other hand, Campbell (1989) observed that slides of the same size but smaller initial fall heights, run out with smaller relative friction coefficient.

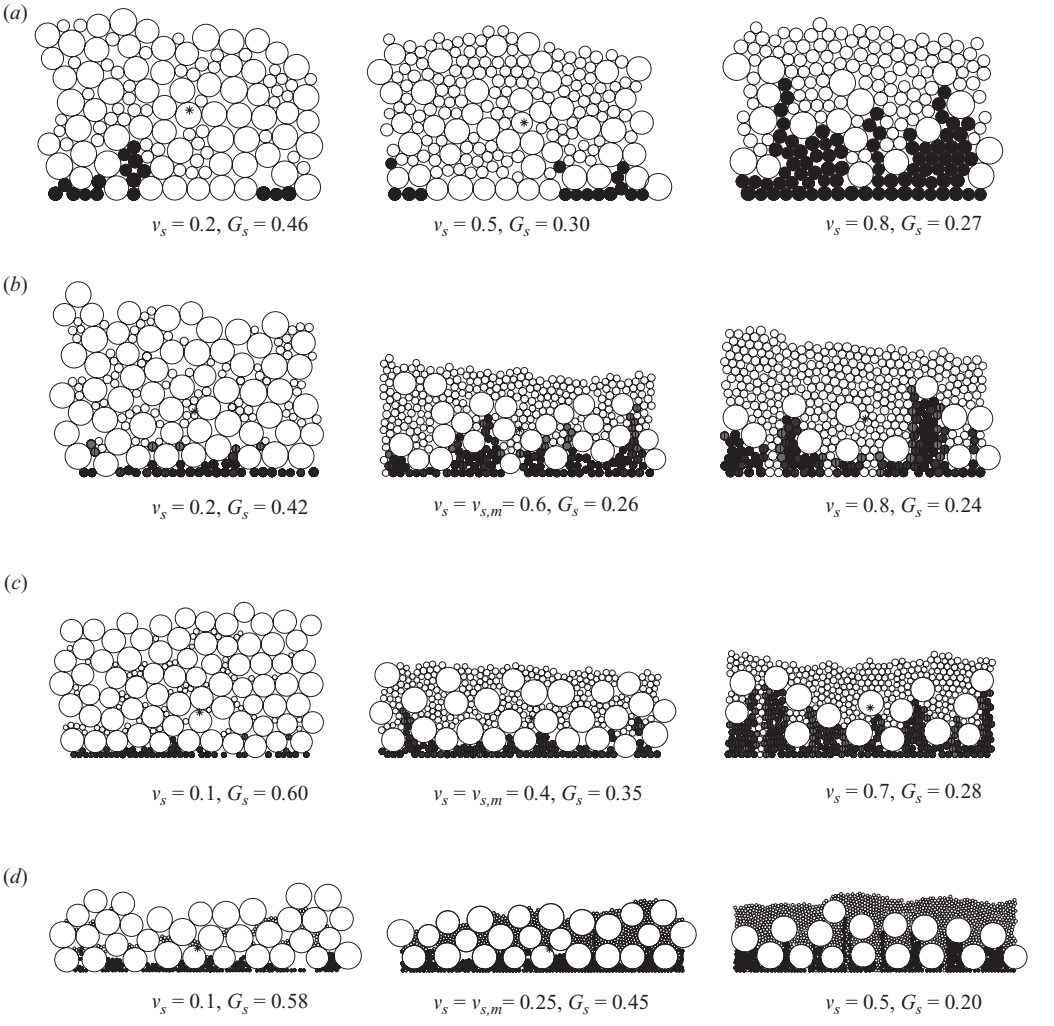

FIGURE 16. Distribution of the small and large particles in the final deposit for different ratios d_l/d_s and for different area fractions of small particles (*a*) $d_l/d_s = 2$, (*b*) $d_l/d_s = 3$, (*c*) $d_l/d_s = 4$, (*d*) $d_l/d_s = 8.3$. The value of the Gini coefficient for small particles, G_s, is indicated in each case.

In order to evaluate the effect of the avalanche fall height on the runout, simulations with different initial bulk heights were conducted for the case of a diameter ratio equal to 3 and an area fraction of small particles equal to 0.60 (corresponding to $\nu_{s,m}$). The initial height of the deposit was changed to vary the travel distance on the inclined plane from 10 d_l to 300 d_l.

The results presented in figure 21 show that the global friction coefficent $\mu = H_{cm}/L_{cm}$ increases with the initial bulk height of the centre of mass (H_i/d_s). This is in agreement with the results obtained by Campbell (1989) for monodisperse avalanche simulations, who attributed the reduction of mobility to an increased stress due to the increment of the avalanche kinetic energy with height. In our case, in addition to the mechanism proposed by Campbell, the increase of the effective friction can also be attributed to the destruction of the basal layer of small particles.

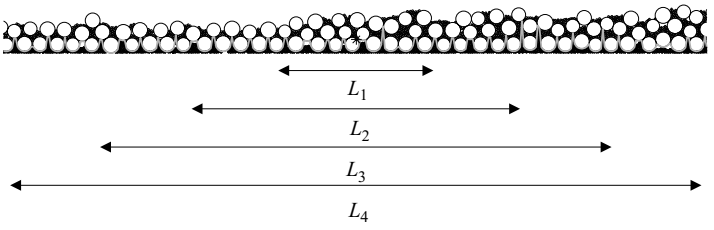

FIGURE 17. The thickness, h_{layer}, was determined for each length L. The reported value is an average of the measurement considering several values of L.

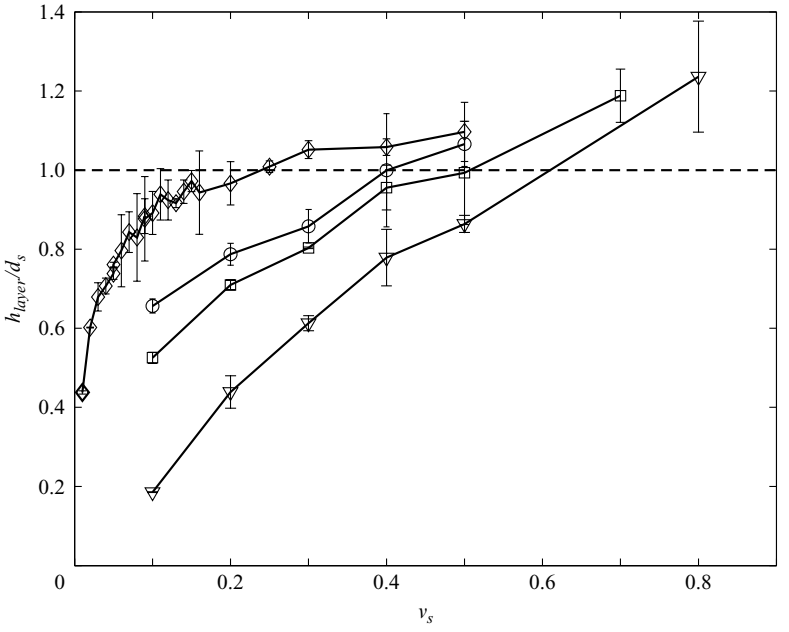

FIGURE 18. Dimensionless thickness of the layer of small beads at the base of the final deposit h_{layer}/d_s as a function of ν_s for different diameter ratios: $\diamond$, $d_l/d_s = 8.3$; $\bigcirc$, $d_l/d_s = 4$; $\square$, $d_l/d_s = 3$; $\triangledown$, $d_l/d_s = 2$.

Figure 22 shows the thickness of the layer of small beads as a function of time for avalanches with different initial heights. It was found that dimensionless thickness of the layer of small beads h_{layer}/d_s decreases with time and tends to the value 1 for large times. Moreover, the curves are classified: there is an increase (for a given time) of the thickness of the layer of small beads with the increase of the initial position.

The mean angular velocity of the small beads touching the plane is presented in figure 23, as a function of time. The rotation increases, reaches a maximum value, decreases and tends to a constant value. The curves for different initial positions are also classified. The maximum of the rotation increases with the initial position. Note that for an increase of the initial position, the thickness of the layer of small beads increases (and is larger than 1), but also the rotation of the small beads increases. These two results give opposite behaviours: an increase of the thickness of the layer of small beads would lead to an increase of the global coefficient of friction, whereas an increase of the rotation would lead to a decrease of the global coefficient of friction. However, since the effective friction was found to increase with the initial

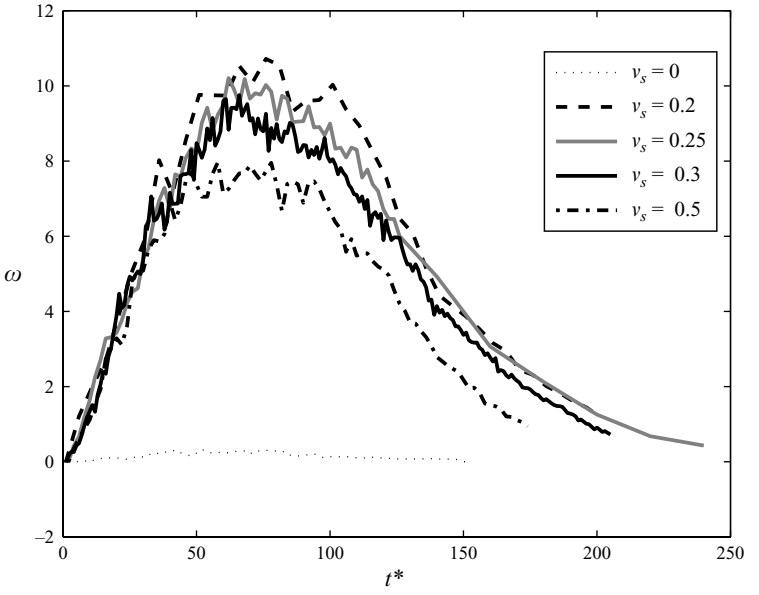

FIGURE 19. Variation of the mean dimensionless angular velocity as a function of dimensionless time for different area fractions of small particles for $d_l/d_s = 8.3$.

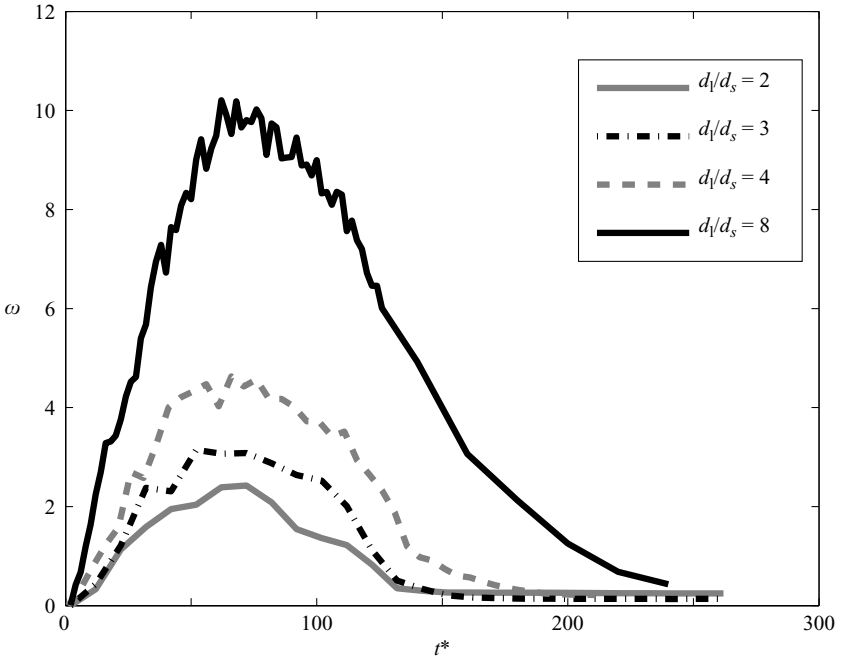

FIGURE 20. Variation of the mean dimensionless angular velocity as a function of dimensionless time for different diameter ratios for $v_{s,m}$.

height, it can be argued that the rolling of beads in the layer has a minor role in this particular case. To understand further the mechanism that leads to the destruction of the basal layer, the compactness for each bead on the basal layer was determined using Voronoï cells. Figure 24 shows the mean compactness of the simulations with

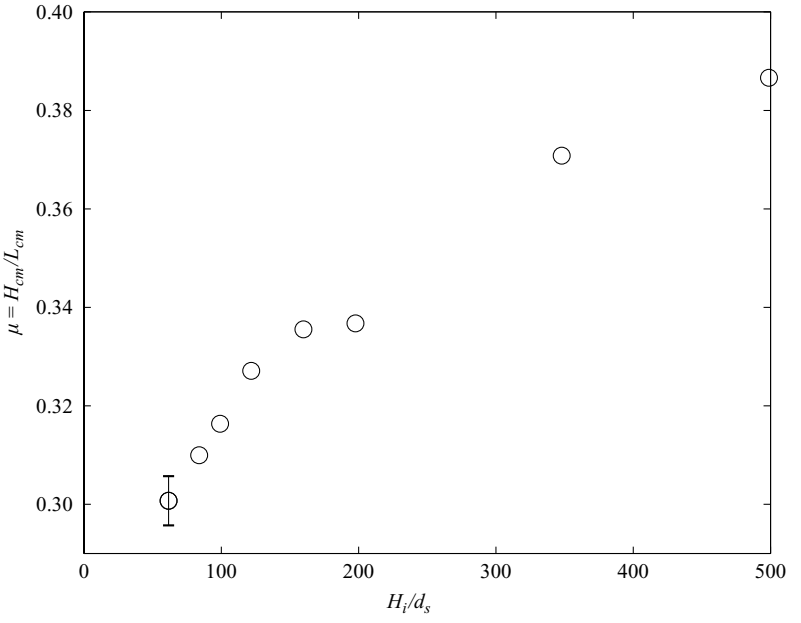

FIGURE 21. The global friction coefficient as a function of the initial dimensionless height (H_i/d_s). For this case $d_l/d_s = 3$ and $\nu_s = 0.60$. The error bar of the first data point denotes the variability found when the simulation was repeated five times for the same nominal conditions.

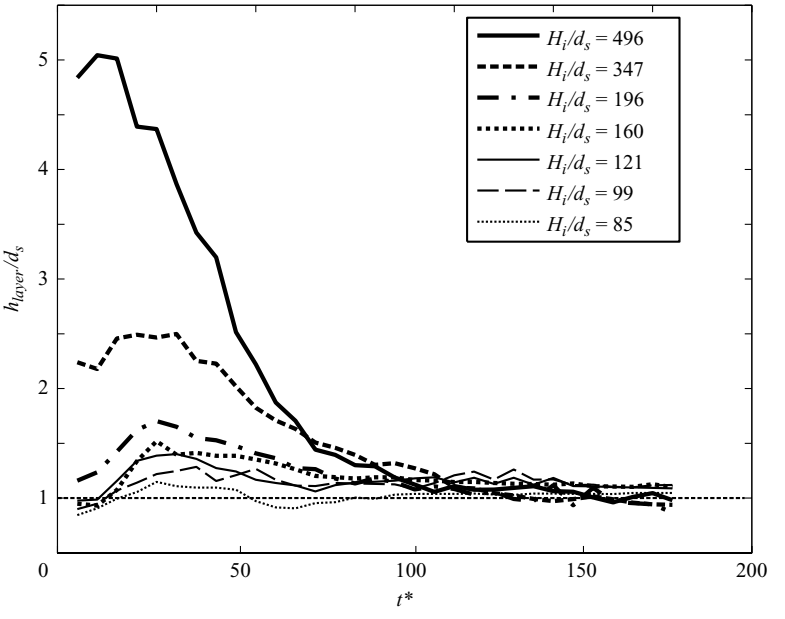

FIGURE 22. Basal layer height variation as a function of dimensionless time for different initial dimensionless heights. The horizontal line corresponds to a basal layer height equal to one.

different initial heights as a function of time. The compactness decreases with the time, reaches a minimum value and increases to reach a value close to 0.74. The minimum of the compactness decreases as the initial height position increases; that is, the decompaction increases with the initial position. In fact, this decompaction

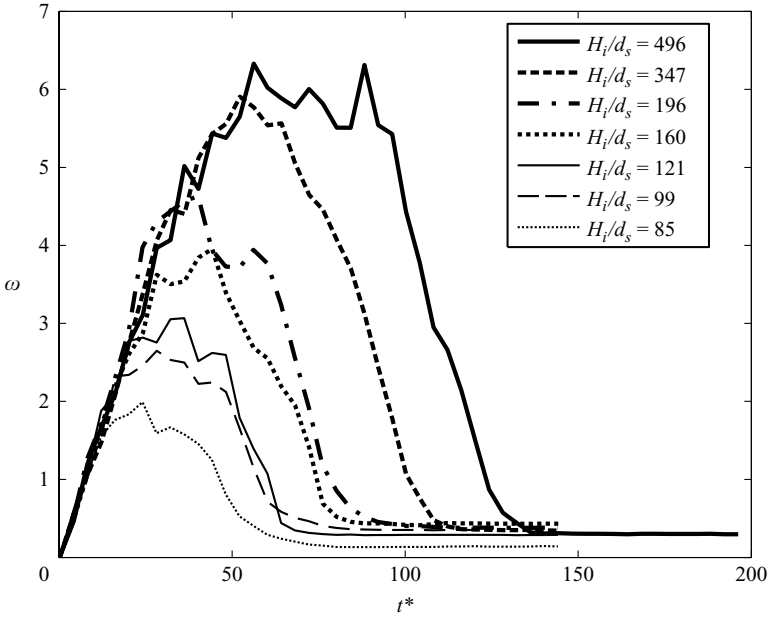

FIGURE 23. Variation of the dimensionless angular velocity as a function of dimensionless time, for different dimensionless initial heights. For this case $d_l/d_s = 3$ and $\nu_s = 0.6$.

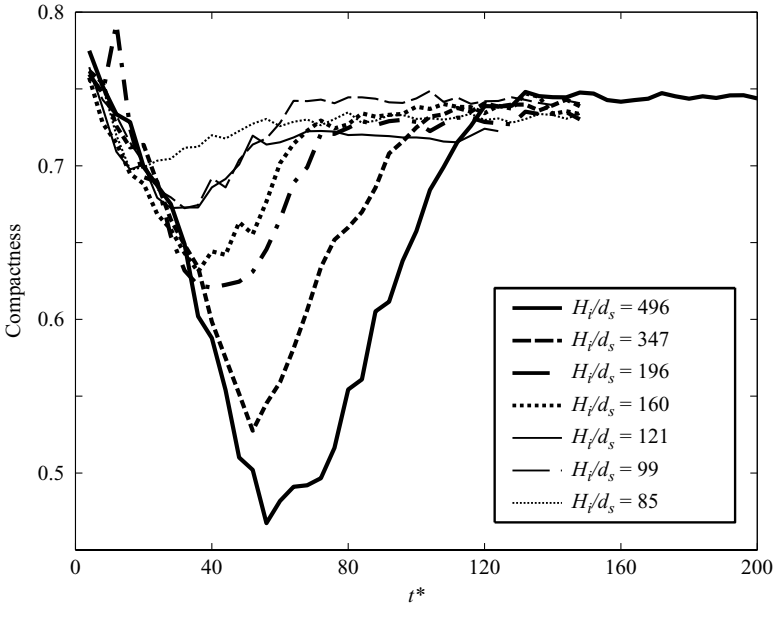

FIGURE 24. Mean compactness as a fucntion of time, for different dimensionless initial heights. For this case $d_l/d_s = 3$ and $\nu_s = 0.6$.

behaviour may be expected since avalanches descending from larger initial heights will gain more kinetic energy; leading to increased agitation and, in turn, decompaction.

It can then be concluded that for this case, the increase of the coefficient of friction with the initial position is due to an increase of the thickness of the basal layer of

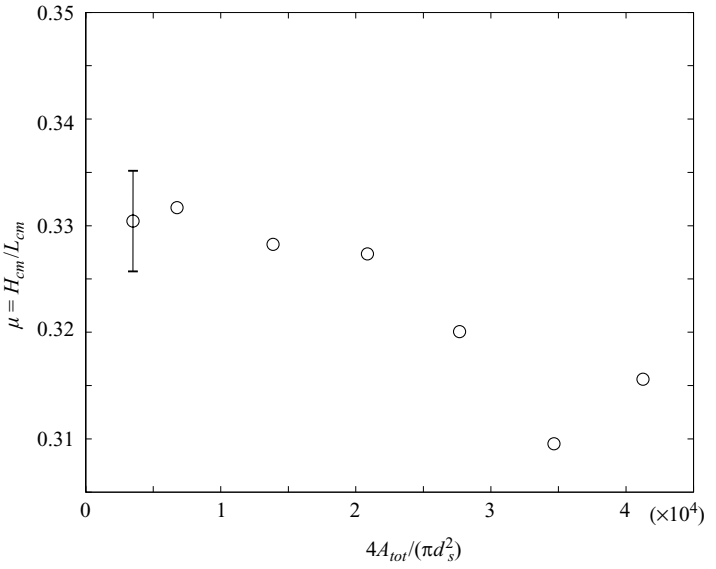

FIGURE 25. Global friction coefficient as a function of dimensionless total area, $4A_{tot}/(\pi d_s^2)$. $d_l/d_s = 3$ and $\nu_s = 0.6$. The error bar of the first data point denotes the variability found when the simulation was repeated for the same nominal conditions.

small beads, and to its decompaction during the avalanche. Moreover, the increased rotation of the small beads, seems not to be sufficient to result in a decrease of the global coefficient of friction.

6. Dependence of runout on the avalanche size

One of the characteristics of long runout landslides is that their effective friction coefficient decreases as the volume of the avalanche increases (Siebert 1984; Self & Hayashi 1992; Sheridian, Siebe & Komorowski 1992). To verify that the mechanism investigated here is also valid for different sizes of avalanches, some simulations were run for a range of initial areas. The diameter ratio for these simulations was chosen to be equal to 3 with an area fraction of small particles equal to 0.60. The global coefficient of friction, H_{cm}/L_{cm}, was found to decrease with the area of the avalanche as shown in figure 25. This result is in qualitative agreement with what is observed for real avalanches. This tendency can also be explained by analysing the basal layer of the avalanche. The dimensionless thickness of the layer of small beads increases with the avalanche area reaching a mean value of 1 when the avalanche is sufficiently large. Figure 26(*a*) shows the measured dimensionless thickness of the basal layer as a function of time for different avalanche sizes. The rotation of the beads at the basal layer is approximately the same for the different avalanche sizes (figure 26*b*), regardless of the observed decrease of the global friction coefficient.

Again, for this case, the global coefficient of friction is a minimum for a thickness of the layer of small beads equal to d_s. The thickness of the layer of small beads increases from 0 (small area) to 1 (large area). Because of similar values of the rotation for all the experiments, the rolling interaction rotation of small beads seems to have no influence in this case. In conclusion, the decrease of the global coefficient of friction with the area is due to an increase of the thickness of the layer of small beads. Our results show a negative correlation between the apparent friction coefficient and the

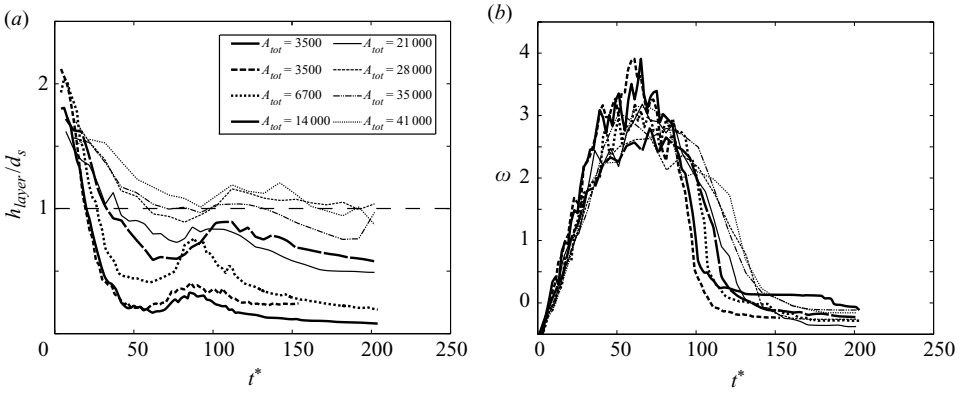

FIGURE 26. (*a*) Dimensionless thickness of the layer of small beads h_{layer}/d_s at the base of the flow as a function of dimensionless time t^*. (*b*) Variation of the basal dimensionless angular velocity as a function of dimensionless time for different areas. For this case, $d_l/d_s = 3$ and $\nu_s = 0.6$.

avalanche size, a tendency observed in large avalanches. However, this trend in real avalanches exhibits a large scatter, which remains controversial (Iverson & Vallance 2001; Legros 2002).

As explained in § 2, the simulations are made dimensionless, considering the diameter of small particles as the characteristic length scale. From the results shown above, it follows that the apparent coefficient of friction in these simulations depends on the number of particles, and not directly on the volume of the avalanche. Consequently, low apparent coefficients of friction should occur for large or small avalanche volumes. Our study predicts an enhanced mobility at all scales provided that a lubricant basal layer of small particles is formed.

7. Conclusions

In summary, simulations were conducted to investigate the effect of a second species of particles on the runout length of granular avalanches. We found that the particle species with small diameter segregates and moves to the base of the flow. The layer of small particles at the base of the flow serves as a lubrication layer that results in a reduction of the global friction coefficient and, hence, an increase of the runout of the avalanche. The layer of small particles changes the frictional dynamics of the avalanche's base from a combination of rolling and sliding contacts to a rolling-dominated interaction. This mechanism is, in fact, the same as used in mechanical ball bearings. The reduction of friction is maximum for a certain area fraction of small particles for which a continuous layer of one diameter is formed at the base of the flow. Moreover, the value of the most efficient area fraction of small beads $\nu_{s,m}$ depends on d_l/d_s having a continuous behaviour. Although, the system studied here is a simplification, we can argue that the same mechanism occurs in real avalanches. All geological granular masses are composed by particles of several sizes and, in fact, small particles are commonly found at the base of the final deposits (Bursik *et al.* 1979; Saucedo, Macías & Bursik 2004). Hence, the effect reported here would increase the mobility of landslides even for a small amount of a small size species. Simulations with different initial height fall and different areas were also performed. These results are in agreement with the results obtained by Campbell (1989) and

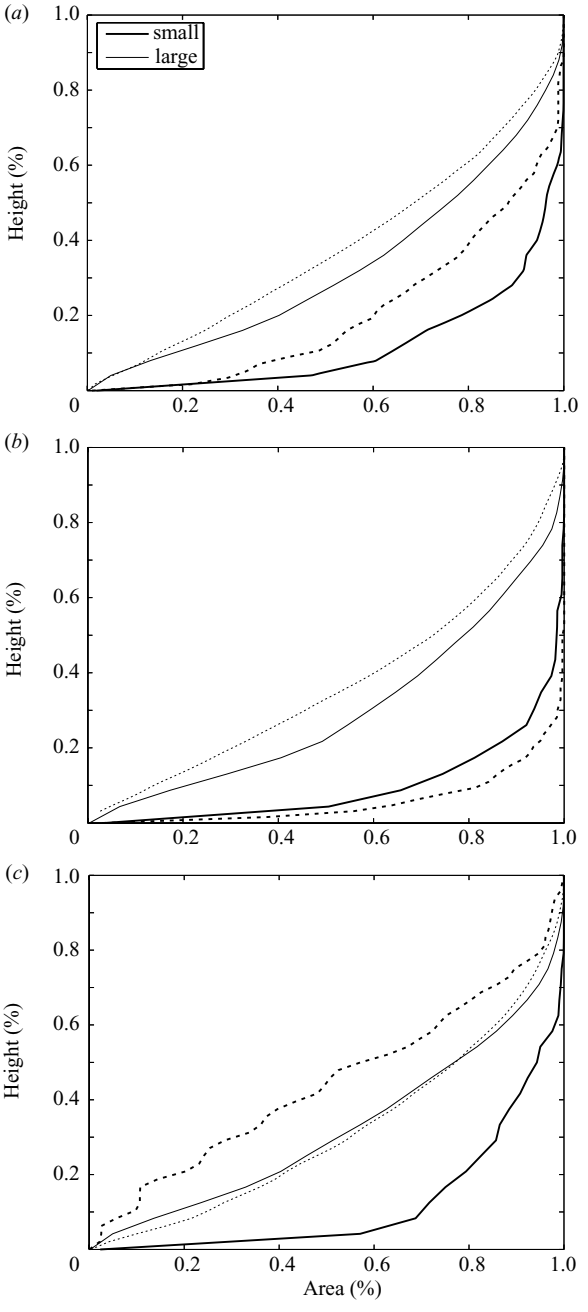

FIGURE 27. Lorenz curve for the three configurations. The dotted lines are for the initial time, and the continuous lines for the final time. (*a*) Well-mixed initial configuration. (*b*) Small beads at the base. (*c*) Small beads at the top.

provide a new insight for explaining this behaviour. The analysis outlined here does not obviously preclude any of the previous explanations for the enhanced mobility of some rock falls. This phenomena is far more complex and there are many factors that contribute to the runout of mass movements of dry debris flows and rocks. However,

ν_s	μ (well mixed)	μ (small at base)	μ (small on top)
0.05	0.364	0.328	0.350
0.20	0.226	0.244	0.240

TABLE 2. Global friction coefficient for three different initial configurations, for two values of ν_s.

our analysis does indicate that geometrical effects in flows containing more than one particle size have important implications in the extent of the runout. Although it is expected that this mechanism is also present in three-dimensional avalanches, the effective lubrication may be different because the segregation rate is much quicker for such flows; hence, the formation of the basal layer would occur more rapidly. Also, in three-dimensions the rotation of the particles would not be unidirectional, so the rolling dynamics may be affected, resulting in a less effective reduction of the friction.

This work was supported by the UNAM research program (PAPIIT grant IN-102303). C. G. acknowledges the support of UNAM's postdoctoral program.

Appendix. Influence of the initial mixture on the segregation

One natural question to ask is whether the initial particle distribution affects the phenomena described in this investigation. To answer this question, we performed a few additional simulations in which a preferential distribution of particles could be imposed on the initial arrangement. For most simulations, small and large particles were placed randomly in an initial region and allowed to settle and accommodate themselves freely (figure 2). The initialization program was modified to locate the small particles separated, either above or below, from the large ones. Hence, preferential initial particle distributions were produced. The three different configurations considered are shown in figure 6. The diameter ratio is equal to 5 and area fractions of small beads of 0.05 and 0.2 were studied.

Figure 27 shows the Lorenz curves for the initial and final deposits considering the three initial configurations. It can be observed that final particle distribution does not seem to be affected by the initial configuration: the Lorenz curves for small and large beads are similar for the different configurations. For the initially well-mixed case, the Gini coefficient for both species increases from the initial to final states, which is an indication of the segregation that occurred during the avalanche. For the case in which the particles are preferentially near the bottom of the initial deposit, the Lorenz curves for the initial and final times remain relatively unchanged. In this case, the granular mass is already segregated and no significant changes of the evolution of the avalanche structure are identified. In the other case, for which the small particles are initially on the top, the shape of the Lorenz curves for small particles changes significantly from beginning to end, depicting a transition from unmixed, mixed and unmixed again. The Gini coefficient is larger in the case where the large beads are at the bottom of the flow than in the case where the small beads are at the bottom of the flow (because in this case no segregation can occur: the mixture is already segregated). More importantly, the global coefficient of friction does not seem to be significantly affected by the initial conditions as shown in table 2 where it can be observed that for the two initially segregated cases (small beads at the top or at the base), the global friction coefficient is approximately the same. For the initially

well-mixed configuration, the effective friction is slightly different from in the two others configurations, but the difference is small, approximately of 7%. Clearly, the initial configuration does not affect the results in a significant manner.

REFERENCES

Aharonov, E. & Sparks, D. E 1999 On phase transition and self-organized critical state in granular packings, *Phys. Rev.* E **60**, 6890.

Balmforth, N. J. & Kerswell, R. R. 2005 Granular collapse in two dimensions. *J. Fluid Mech.* **538**, 399–428.

Barber, C. B., Dobkin, D. P. & Huhdanpaa, H. T. 1996 The quickhull algorithm for convex hulls. *ACM Trans. Math. Software* **22**, 469–483.

Bates, R. L. & Jackson, J. A. 1962 *Dictionary of Geological Terms.* American Geological Institute, Anchor Books.

Bridgwater, J. 1976 Fundamental powder mixing mechanisms. *Powder Technol.* **15**, 215–236.

Bursik, M., Patra, A., Pitman, E. B., Nichita, C., Macías, J. L., Saucedo, R. & Girina, O. 1979 Advances in studies of dense volcanic granular flows. *Rep. Prog. Phys.* **68**, 271–301.

Campbell, C. S. 1989 Self-lubrication for long runout landslides. *J. Geol.* **97**, 653–665.

Campbell, C. S., Cleary, P. W. & Hopkins, M. 1995 Large-scale landslide simulations: global deformation, velocities and basal friction. *J. Geophys. Res.* **100**, 8267–8283.

Cleary, P. W. & Campbell, C. S. 1993 Self-lubrication for long-runout landslides: examination by computer simulations. *J. Geophys. Res.* **100**, 21 911–21 924.

Cundall, P. A. & Strack, O. D. L. 1979 A discrete numerical model for granular assemblies. *Geotechnique* **29**, 47–65.

Dade, W. B. & Huppert, H. E. 1998 Long runout rockfalls. *Geology* **26**, 803–806.

Davies, T. R. H. 1982 Spreading of rock avalanche debris by mechanical fluidization. *Rock Mech.* **15**, 9–24.

Dolgunin, V. N. & Ukolov, A. A. 1995 Segregation modelling of particle rapid gravity flow. *Powder Technol.* **83**, 95–103.

Drahun, J. A. & Bridgwater, J. 1983 The mechanisms of free surface segregation. *Powder Technol.* **36**, 39–53.

Ehrichs, E. E., Jaeger, M. M., Karezmar, G. S., Knight, J. B., Kuperman, V. Y. & Nager, S. R. 1995 Granular convection observed by magnetic-resonance-imaging. *Science* **267**, 1632–1634.

Fahnestock, R. K. & Voight, B. (ed.) 1978 *Rockslides and Avalanches. 1. Natural phenomena.* Elsevier.

Gary, M., McAffe, R. & Wolf, C. L. 1972 Glossary of Geology: Washington, D.C. *Am. Geol. Inst.* 805.

Gastwirth, J. L. 1972 The estimation of the Lorenz curve and Gini index. *Rev. Econ. Stat.* **54**, 306–316.

Gini, C. 1912 Variabilità e mutabilità. Reprinted in *Memorie di metodologica statistica* (ed. E. Pizetti & T. Salvemini). Libreria Eredi Virgilio Veschi, Rome (1955).

Goujon, C., Dalloz-Dubrujeaud, B. & Thomas, N. 2007 Bidisperse granular avalanches on inclined rough planes: a rich variety of behaviors. *Eur. Phys. J.* E **23**, 199–215.

Gray, J. M. N. T. & Chugunov, V. A. 2006 Particle-size segregation and diffusive remixing in shallow granular avalanches. *J. Fluid Mech.* **569**, 365–398.

Gray, J. M. N. T. & Thornton, A. R. 2005 A theory for particle size segregation in shallow granular free-surface flows. *Proc. R. Soc. Lond.* A **461**, 1447–1473.

Heim, A. 1932 Bergsturz und Menschenleben. *Vierteljahresschrift Naturf. Ges. Zürich* **77**, 1218.

Howard, K. 1973 Avalanche mode of motion: implications from lunar examples. *Science* **180**, 1052–1055.

Hsiau, S. S. & Hunt, M. L. 1993 Shear-induced particle diffusion and longitudinal velocity fluctuations in a granular-flow mixing layer. *J. Fluid. Mech.* **251**, 299–313.

Hsü, K. J. 1975 Catastrophic debris streams (Sturzstroms) generated by rockfalls. *Geol. Soc. Am. Bull.* **86**, 129–140.

Hungr, O. & Evans, S. G. 1997 A dynamic model for landslides with changing mass. *Engng. Geol. Environ.* **41**, 719–722.

Huppert, H. E. & Dade, W. B. 1998 Natural disasters: explosive volcanic eruptions and gigantic landslides. *Theoret. Comput. Fluid Dyn.* **10**, 201–212.

Iverson, R. M. & Vallance, J. W. 2001 New views of granular mass flows. *Geolog. Soc. Am.* **29**, 115–118.

Jenkins, J. T. 1998 Particle segregation in collisional flows of inelastic spheres. In *Physics of Dry Granular Media* (ed. H. J. Herrmann, J.-P. Hovi & S. Luding), pp. 645–658. NATO ASI series, Kluwer.

Jullien, R., Meakin, P. & Pavlovitch, A. 1992 Three dimensional model for particle size segregation by shaking. *Phys. Rev. Lett.* **69**, 640–643.

Kent, P. E. 1966 The transport mechanism in catastrophic rock falls. *J. Geol.* **74**, 79–83.

Lajeunesse, E., Mangeney-Castelnau, A. & Vilotte, J. P. 2004 Spreading of a granular mass on a horizontal plane. *Phys. Fluids* **16**, 2371–2381.

Lajeunesse, E., Quantin, C., Allemand, P. & Delacourt, C. 2006 New insights on the runout of large landslides in the Valles-Marineris Canyons, Mars. *Geophys. Res. Lett.* **33**, 4403.

Legros, F. 2002 The mobility of long-runout landslides. *Engng. Geol.* **63**, 301–331.

Lorenz, M. O. 1905 Methods of measuring the concentration of wealth. *Publ. Am. Stat. Assoc.* **9**, 209–219.

Lube, G., Huppert, H. E., Sparks, R. S. J. & Hallworth, M. A. 2004 Axisymmetric collapses of granular columns. *J. Fluid Mech.* **508**, 175–199.

Lun, C. K. K. & Bent, A. A. 1994 Numerical simulation of inelastic frictional spheres in simple shear flow. *J. Fluid Mech.* **258**, 335–353.

Melosh, H. J. 1979 Acoustic fluidization–a new geologic process? *J. Geophys. Res.* **84**, 7513–7520.

Phillips, J. C., Hogg, A. J., Kerswell, R. R. & Thomas, N. H. 2006 Enhanced mobility of granular mixtures of fine and coarse paricles. *Earth Planet. Sci. Lett.* **246**, 466–480.

Poschel, T. & Buchholtz, V. 1979 Static friction phenomena in granular materials: Coulomb law versus particle geometry. *Phys. Rev. Lett.* **71**, 3963–3966.

Rosato, A., Strandburg, K. J., Prinz, F. & Swendsen, R. H. 1987 Why the brazil nuts are on top: size segregation of particulate matter by shaking. *Phys. Rev. Lett.* **58**, 1038–1040.

Rotter, J. M., Holst, F. G., Ooi, J. Y. & Sanad, A. M. 1998 Silo pressure predictions using discrete-element and finite-element analyses. *Phil. Trans. R. Soc. Lond.* A **356**, 2685–2712.

Saucedo, R., Macías, J. L. & Bursik, M. 2004 Pyroclastic flow deposits of the 1991 eruption of Volcan de Colima, Mexico. *Bull. Volcanol.* **66**, 291–306.

Savage, S. B. 1989 Flow of granular materials. In *Theoretical and Applied Mechanics* (ed. P. Germain, M. Piau & D. Caillerie), pp. 241–266. Elsevier.

Savage, S. B. & Dai, R. 1993 Studies of granular shear flows. Wall slip velocities, layering and self-diffusion. *Mech. Mat.* **16**, 225–238.

Savage, S. B. & Hutter, K. 1989 The motion of a finite mass of granular material down a rough incline. *J. Fluid Mech.* **199**, 177–215.

Savage, S. B. & Lun, C. K. K. 1988 Particle size segregation in inclined chute flow of dry cohesionless granular solids. *J. Fluid. Mech.* **189**, 311–335.

Schafer, J., Dippel, S. & Wolf, D. E. 1996 Force schemes in simulations of granular materials. *J. Phys.* I *France* **6**, 5–20.

Scheidegger, A. E. 1975 *Physical Aspects of Natural Catastrophes.* Elsevier.

Self, S. & Hayashi, J. N. 1992 A comparison of pyroclastic flow and landslide mobility. *J. Geophys.* **97**, 9063–9071.

Shaller, P. J. & Smith-Shaller, A. 1996 Sturzstroms and detachment faults. In *Anbza-Borrego Desert State Park, California South Coast Geol. Soc.* (ed. P. L. Abott & D. C. Semour), pp. 185–202. Santa Anna.

Sheridian, M. F., Siebe, C. & Komorowski, J. C. 1992 Morphology and emplacement of unusual debris–avalanche deposit at Jocotitlán volcano. *Bull. Volcanol.* **54**, 573–589.

Shreve, R. L. 1968 The Blackhawk landslide. *Geol. Soc. Am. Bull.* **79**, 653–658.

Siavoshi, S., Orpe, A. V. & Kudrolli, A. 2006 Friction of a slider on a granular layer: nonmonotonic thickness dependence and effect of boundary conditions. *Phys. Rev. E* **73**, 010301.

Siebert, L. 1984 Large volcanic debris avalanches: characteristics of source areas, deposits and associated eruptions. *J. Volcanol. Geotherm.* **22**, 163–197.

Straub, S. 1996 Self-organisation in the rapid flow of granular material: evidence for a major flow mechanism. *Geol. Rundsch.* **85**, 85–91.

Thomas, N. 2000 Reverse and intermediate segregation of large beads in dry granular media. *Phys. Rev.* E **62**, 961–974.

Thornton, A. R., Gray, J. M. N. T. & Hogg, A. J. 2006 A three-phase mixture theory for particle size segregation in shallow granular free-surface flows. *J. Fluid Mech.* **550**, 1–25.

Vallance, J. W. & Savage, S. B. 2000 Particle segregation in granular flows down chute. In *IUTAM Symp. on segregation in granular materials* (ed. A. D. Rosato & D. L. Blackmore), pp. 3151. Kluwer.

Walton, O. R. & Braun, R. L. 1986 Viscosity, granular-temperature, and stress calculations for shearing assemblies of inelastic, frictional disks. *J. Rheol.* **30**, 949–980.

Wassgren, C. R. 1996 Vibration of granular materials. PhD thesis, California Institute of Technology.

Zenit, R. 2005 Computer simulations of the collapse of a granular column. *Phys. Fluids* **17**, 031703.